Compilation of non-linear three-component model for simulations of rate-dependent load-strain-time behaviours of geogrids

Yodphao Punya-in & Warat Kongkitkul
King Mongkut's University of Technology Thonburi, Thailand

ABSTRACT: Polymer geosynthetic reinforcements show the elasto-visco-plastic load-strain-time behaviours, which have been revealed by many past tensile loading test results. These behaviours can be accurately described using a non-linear three-component (NTC) model, especially when subjected to complex loading histories including, for example, changes in the strain rate, creep, stress relaxation, etc. Two viscosity types, Isotach and Combined, have been found relevant for various geosynthetic reinforcements. In this paper, the equilibrium equations of the NTC model for geosynthetic reinforcements are described and the algorithms for utilising them for simulations of load-strain-time behaviours are detailed. Three simulation modes consisted of constant-strain-rate monotonic loading, sustained loading and stress relaxation are presented. Aiming to encourage the use of the NTC model by other researchers, a work example in Microsoft Excel with a user-defined Microsoft Visual Basic source code is also provided.

Keywords: geosynthetic, rate-dependent, elasto-visco-plastic, non-linear three-component model, monotonic loading, creep loading, load relaxation

1 INTRODUCTION

As geosynthetic reinforcements are made of polymer, their load-strain-time behaviours have been among serious engineering concerns, which led to a number of systematic studies in the past. These studies revealed that geosynthetic reinforcements exhibit: i) dependency of the rupture tensile strength on the strain rate, ii) creep deformation under sustained constant loading, iii) load relaxation at a fixed strain, and iv) tensile load jump upon a step increase or decrease in the strain rate. These facts imply that the load-strain-time behaviours of polymer geosynthetic reinforcements are rate-dependent. These trends of rate-dependent behaviour were successfully simulated with a non-linear three-component (NTC) model (e.g., Hirakawa et al. 2003, Kongkitkul et al. 2004, 2007a, 2007b, 2010, 2014, Ezzein et al. 2015, Shi et al. 2016) (Figure 1a). By the framework of NTC model, Tatsuoka et al. (2008) showed that, for geomaterials (i.e., soils and rocks), there are four basic viscosity types, which are Isotach, Combined, TESRA, and P&N (Figure 1b). For geosynthetic reinforcements, most of them exhibit Isotach viscosity, while only with PET geogrid the Combined viscosity (Hirakawa et al. 2003).

The implementation of NTC model was limited to self-coding computer program (e.g., Ishihara 2000, Nishi 2002). It was implemented into MS Excel using VB code for the first time by Kongkitkul et al. (2014), aiming to help the readers to understand how the model works so that they can further modify the code for their specific problems. The code and simulations are, however, limited only to Isotach viscosity, although various loading histories including changes in the strain rate, creep, and stress relaxation were included. In view of the above, the present study aims at development of algorithms and VB source code for MS Excel for more general viscosity types to fulfil the ability of NTC model. Simulations of load-strain-time relations of geogrids that exhibit Isotach and Combined viscosities are also presented.

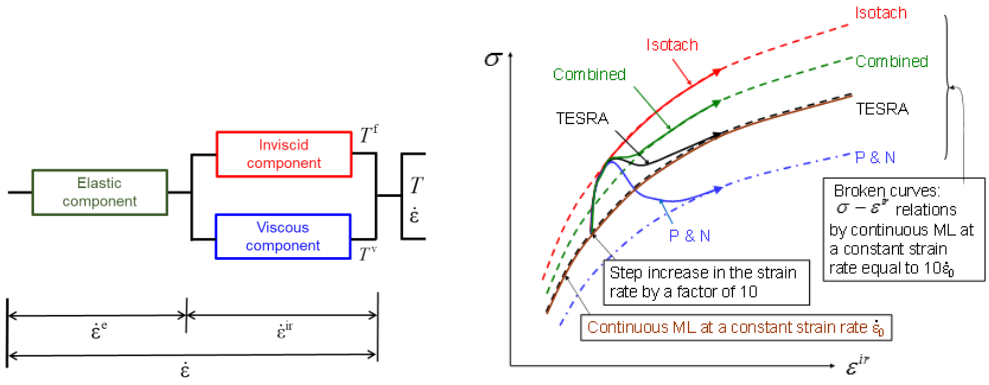

Figure 1. a) Non-linear three-component model modified for polymer geosynthetic reinforcement (modified from Hirakawa et al. 2003); and b) Four basic viscosity types of geomaterials (modified from Tatsuoka et al. 2008)

2 CONSTITUTIVE MODEL OF NON-LINEAR THREE-COMPONENT MODEL

A NTC model (Figure 1a) was used to simulate the load-strain-time behaviours of geosynthetic reinforcements (e.g., Hirakawa et al. 2003, Kongkitkul et al. 2004, Kongkitkul et al. 2007a, Peng et al., 2010, Kongkitkul et al. 2014, Chantachot et al. 2016). As this issue is explained very in details in the literature, only the core of the theory is explained below.

The model consists of three components, i.e., elastic, inviscid, and viscous components (Figure 1a). Tensile load (T) is decomposed into inviscid load (T^f) and viscous load (T^v), while strain rate ($\dot{\varepsilon}$) into elastic strain rate ($\dot{\varepsilon}^e$) and irreversible strain rate ($\dot{\varepsilon}^{ir}$), as follows:

$$T = T^f + T^v \tag{1a}$$

$$\dot{\varepsilon} = \dot{\varepsilon}^e + \dot{\varepsilon}^{ir} \tag{1b}$$

2.1 *Elastic component*

Elastic strain rate ($\dot{\varepsilon}^e$) is determined using a hypo-elastic model. In so doing, the equivalent elastic stiffness (k_{eq}) is a function of instantaneous tensile load (T) as:

$$\dot{\varepsilon}^e = \dot{T} / k_{eq}(T) \tag{2a}$$

where: $\dot{T}$ is the tensile load rate; and $k_{eq}(T)$ is the tensile load-dependent tangential stiffness (Hirakawa et al. 2003, Kongkitkul et al. 2004, 2007a, 2012) that can be expressed as:

$$k_{eq}(T) = k_{eq0}(T / T_0)^b \tag{2b}$$

where: T_0 is the reference tensile load; k_{eq0} is the value of k_{eq} when $T = T_0$; and b is a constant.

2.2 *Inviscid component*

The inviscid load component (T^f) is expressed as a function of irreversible strain (ε^{ir}) (Di Benedetto et al. 2002, Tatsuoka et al. 2002, 2008). The T^f - ε^{ir} relation, which is also called the "reference load-strain curve", is highly nonlinear for most geosynthetic reinforcements. Generally, it is recommended to use the polynomial function (Hirakawa et al. 2003) as follows:

$$T^f = \sum_{j=1}^{9} a_j \cdot (\varepsilon^{ir})^j \tag{3}$$

where: a_j *(j = 1 to 9)* is the coefficient for term j.

2.3 *Viscous component*

The viscous load (T^v) is generally a function of current irreversible strain (ε^{ir}), its rate ($\dot{\varepsilon}^{ir}$), and strain history (h_s), depending on viscosity type as described below.

2.3.1 *Isotach viscosity*

With Isotach viscosity, the stress jump upon the strain rate change is persistent when the irreversible strain increase (Figure 1b). The Isotach viscous load (T^{v}_{iso}) is a function of instantaneous ε^{ir} and $\dot{\varepsilon}^{ir}$, while independent of h_s as follows:

$$T^{v}_{iso}(\varepsilon^{ir},\dot{\varepsilon}^{ir}) = T^{f}(\varepsilon^{ir})\cdot g_{v}(\dot{\varepsilon}^{ir}) \tag{4a}$$

where: T^{f} is inviscid load (Eq.(3)); and g_v is viscosity function which can be expressed as follows:

$$g_{v}\left(\dot{\varepsilon}^{ir}\right) = \alpha\cdot\left[1-\exp\left\{1-\left(\left|\dot{\varepsilon}^{ir}\right|/\dot{\varepsilon}^{ir}_{r}+1\right)^{m}\right\}\right](\geq 0) \tag{4b}$$

where: α, m and $\dot{\varepsilon}^{ir}_{r}$ are the positive material constants depending on polymer type.

2.3.2 *TESRA viscosity*

With TESRA viscosity type, the stress jump by a stepwise change in the strain rate decays with an increase in ε^{ir} eventually approaches zero (Figure 1b). The TESRA viscosity load (T^{v}_{TESRA}) can be expressed as:

$$T^{v}_{TESRA}(\varepsilon^{ir},\dot{\varepsilon}^{ir},h_s) = \int_{\tau=\varepsilon^{ir}_{1}}^{\varepsilon^{ir}}\left[\mathrm{d}T^{v}_{iso}\right]_{(\tau)}\cdot\left[r(\varepsilon^{ir})\right]^{\left(\varepsilon^{ir}-\tau\right)} \tag{5a}$$

where: $\mathrm{d}T^{v}_{iso}$ can be determined by differentiating Eq.(4a); ε^{ir}_{1} is ε^{ir} at the start of loading where the viscous effect is zero; τ is ε^{ir} at which the viscous load increment $\left[\mathrm{d}V^{v}_{iso}\right]_{(\tau)}$ takes place; and $[r(\varepsilon^{ir})]^{(\varepsilon^{ir}-\tau)}$ is a positive constant lower than unity called the decay function. The $r(\varepsilon^{ir})$ can be expressed as follows:

$$r(\varepsilon^{ir}) = \frac{r_i+r_f}{2}+\frac{r_i-r_f}{2}\cos\left[\pi\cdot\left(\frac{\varepsilon^{ir}}{c}\right)^{n}\right],\ \text{for } \varepsilon^{ir}\geq c:\ r(\varepsilon^{ir}) = r_f \tag{5b}$$

where: r_i, r_f, c and n are material constants. The complex integral form of Eq. (5a) can be approximated by the incremental form (Tatsuoka et al. 2008) as follows:

$$T^{v}_{TESRA}(\varepsilon^{ir},\dot{\varepsilon}^{ir},h_s) \approx \left(T^{v}_{TESRA}\right)_{i}\cdot\left(r(\varepsilon^{ir})\right)^{\Delta\varepsilon^{ir}} + \Delta T^{v}_{iso}(\varepsilon^{ir},\dot{\varepsilon}^{ir})\cdot\left(r(\varepsilon^{ir})\right)^{\Delta\varepsilon^{ir}/2} \tag{5c}$$

2.3.3 *Combined viscosity*

With Combined viscosity, similar to TESRA viscosity, the stress jump by a step change in the strain rate decays with the increasing ε^{ir}. However, the decayed stress jump is only partially (Figure 1b). It can be described that the combined viscous load (T^{v}_{com}) consists of T^{v}_{iso} and T^{v}_{TESRA}, which can be expressed as:

$$T^{v}_{com}(\varepsilon^{ir},\dot{\varepsilon}^{ir},h_s) = \theta(\varepsilon^{ir})\cdot T^{v}_{iso}(\varepsilon^{ir},\dot{\varepsilon}^{ir}) + [1-\theta(\varepsilon^{ir})]\cdot T^{v}_{TESRA}(\varepsilon^{ir},\dot{\varepsilon}^{ir},h_s) \tag{6a}$$

where $\theta(\varepsilon^{ir})$ is the combined parameter which can be expressed as:

$$r(\varepsilon^{ir}) = \frac{\theta_i+\theta_f}{2}+\frac{\theta_i+\theta_f}{2}\cos\left[\pi\times\left(\frac{\varepsilon^{ir}}{\varepsilon^{ir}_{\theta}}\right)^{n_\theta}\right],\ \text{for } \varepsilon^{ir}\geq\varepsilon^{ir}_{\theta}:\ \theta(\varepsilon^{ir}) = \theta_f \tag{6b}$$

where: θ_i, θ_f, $\varepsilon^{ir}_{\theta}$ and n_θ are material constants. When θ = 1.0, Eq.(6a) returns to Eq.(4a) for Isotach viscosity, and when θ = 0, returns to Eq.(5c) for TESRA viscosity. Hence, the viscous load for all viscosity types can be expressed in a general form as follows:

$$T^{v}(\varepsilon^{ir},\dot{\varepsilon}^{ir},h_s) = \theta(\varepsilon^{ir})\cdot T^{v}_{iso}(\varepsilon^{ir},\dot{\varepsilon}^{ir}) + [1-\theta(\varepsilon^{ir})]\cdot T^{v}_{TESRA}(\varepsilon^{ir},\dot{\varepsilon}^{ir},h_s) \tag{6c}$$

3 IMPLEMENTATION OF EQUILIBRIUM EQUATIONS AND ALGORITHM

Simulation can be performed incrementally. That is, suppose that the values at the current stage i are known. Then the values at next step, stage i + 1 (unknown) can be obtained by iterating $\dot{\varepsilon}^{ir}$ so that its value

satisfies convergence of an equilibrium equation at stage $i + 1$ (n.b., selection of the equations depends on simulation mode; ML, SL, SR where: ML = monotonic loading, SL = sustained loading, and SR = stress relaxation). By repeating this procedure from the start of loading, the full time histories of all variables can be obtained. It can be postulated that the iteration of $\dot{\varepsilon}^{ir}$ is the main key of this model. As a result, all the equilibrium equations are expressed in terms of $\dot{\varepsilon}^{ir}$ with subscript [i] and [$i + 1$] for the stages i and $i + 1$, in order to compile for a computational source code and make easy understanding.

3.1 *Expressions of equilibrium equations*

Suppose that stage i is already in equilibrium. Now the value of $\dot{\varepsilon}^{ir}$ that satisfies the equilibrium equations at stage $i + 1$ is to be determined. Tensile load equilibrium at stage $i + 1$ can be derived from Eq.(1). The total load T can be determined either from the elastic component (T^e) or summation of T^f and T^v (Figure 1a), as follows.

$$T_{[i+1]} = T^e_{[i+1]} \tag{7a}$$

$$T_{[i+1]} = T^f_{[i+1]} + T^v_{[i+1]} \tag{7b}$$

T^e at stage i +1 can be determined from T^e at stage i added by tensile load increment as follows.

$$T^e_{[i+1]} = T^e_{[i]} + k_{eq\,[i+1]} \cdot (\dot{\varepsilon}_{[i+1]} - \dot{\varepsilon}^{ir}_{[i+1]}) \cdot dt_{[i+1]} \tag{8}$$

T^f at stage $i + 1$ can be calculated from Eq.(3):

$$T^f_{[i+1]} = \sum_{j=1}^{9} a_j \cdot \left(\varepsilon^{ir}_{[i]} + \dot{\varepsilon}^{ir}_{[i+1]} \cdot dt_{[i+1]}\right)^j \tag{9}$$

T^v at stage $i + 1$ can be determined from Eq.(6c), Eq.(4a), Eq.(4b), Eq.(5b), Eq.(5c), respectively:

$$T^v_{[i+1]} = \theta_{[i+1]} \cdot T^v_{iso\,[i+1]} + [1 - \theta_{[i+1]}] \cdot T^v_{TESRA\,[i+1]} \tag{10a}$$

$$T^v_{iso\,[i+1]} = T^f_{[i+]} \cdot g_{v\,[i+1]};\; g_{v\,[i+1]} = \alpha \cdot [1 - \exp\{1 - (\left|\dot{\varepsilon}^{ir}_{[i+1]}\right| / \dot{\varepsilon}^{ir}_r + 1)^m\}] \tag{10b}$$

$$T^v_{TESRA\,[i]} = T^v_{TESRA\,[i]} \cdot r(\varepsilon^{ir}_{[i+1]})^{\Delta\varepsilon^{ir}} + [\Delta T^v_{iso\,[i+1]}] \cdot (\varepsilon^{ir}_{[i+1]})^{\Delta\varepsilon^{ir}/2};\; \Delta T^v_{iso\,[i+1]} = T^v_{iso\,[i+1]} - T^v_{iso\,[i]} \tag{10c}$$

3.2 *Solving OF EQUILIBRIUM EQUATIONS AND ALGORITHM*

For each mode of simulation, two equilibrium equations are prepared for: i) $T = T^e$ (feq_1), and ii) $T = T^f + T^v$ (feq_2). These equilibrium equations are expressed in terms of $\dot{\varepsilon}^{ir}_{[i+1]}$. Then they are solved for $\dot{\varepsilon}^{ir}_{[i+1]}$ that satisfies $T = T^e = T^f + T^v$, of which the following condition is satisfied.

$$f(\dot{\varepsilon}^{ir}_{[i+1]}) = feq_1(\dot{\varepsilon}^{ir}_{[i+1]}) - feq_2(\dot{\varepsilon}^{ir}_{[i+1]}) \approx 0 \tag{11}$$

After setting the above-mentioned condition, an iteration process shown in the flowchart (Figure 2) is required to find the root. Figure 2 shows algorithm used in the simulation described in the present study. Bisection method was implemented to find $\dot{\varepsilon}^{ir}_{[i+1]}$ that make convergence at stage $i + 1$, which can be satisfied when $f(\dot{\varepsilon}^{ir}_{[i+1]})$ approximately to zero or is smaller than 10^{-5} % or other values set by the user.

There are three simulation modes implemented (i.e., ML, SL, and SR). Simulation in each mode requires two equilibrium equations as described earlier. For simulation in ML and SR modes, the total strain rate $\dot{\varepsilon}^{ir}_{[i+1]}$ is used as driving parameter for the reasons that: i) $\dot{\varepsilon}^{ir}_{[i+1]}$ is constant for a time interval in ML mode; and ii) $\dot{\varepsilon}^{ir}_{[i+1]}$ is zero for SR mode for a time interval. By substituting Eq.(7b) and Eq.(8) into feq_1 and feq_2 of Eq.(11), the following equilibrium equations are obtained.

$$feq_{ML-1}(\dot{\varepsilon}^{ir}_{[i+1]}) = feq_{SR-1}(\dot{\varepsilon}^{ir}_{[i+1]}) = T^e_{[i+1]} \tag{12a}$$

$$feq_{ML-2}(\dot{\varepsilon}^{ir}_{[i+1]}) = feq_{SR-2}(\dot{\varepsilon}^{ir}_{[i+1]}) = T^{f}_{[i+1]} + T^{v}_{[i+1]} \quad (12b)$$

$$f_{ML}(\dot{\varepsilon}^{ir}_{[i+1]}) = f_{SR}(\dot{\varepsilon}^{ir}_{[i+1]}) = T^{e}_{[i]} - (T^{f}_{[i+1]} + T^{v}_{[i+1]}) \approx 0 \quad (12c)$$

For SL mode, as the total load for a time interval does not change, the total loads at the previous and current stages are the same, and thus, the following can be expressed: $feq_1(\dot{\varepsilon}^{ir}_{[i+1]}) = T_{[i]}$ and $feq_2(\dot{\varepsilon}^{ir}_{[i+1]}) = T_{[i+1]}$. In the present study, $T_{[i]}$ and $T_{[i+1]}$ are obtained from T^e and $T^e + T^v$, respective, as follows.

$$feq_{SL-1}(\dot{\varepsilon}^{ir}_{[i+1]}) = T^{e}_{[i]} \quad (13a)$$

$$feq_{SL-2}(\dot{\varepsilon}^{ir}_{[i+1]}) = T^{f}_{[i+1]} + T^{v}_{[i+1]} \quad (13b)$$

$$f_{SL-2}(\dot{\varepsilon}^{ir}_{[i+1]}) = T^{e}_{[i]} - (T^{f}_{[i+1]} + T^{v}_{[i+1]}) \approx 0 \quad (13c)$$

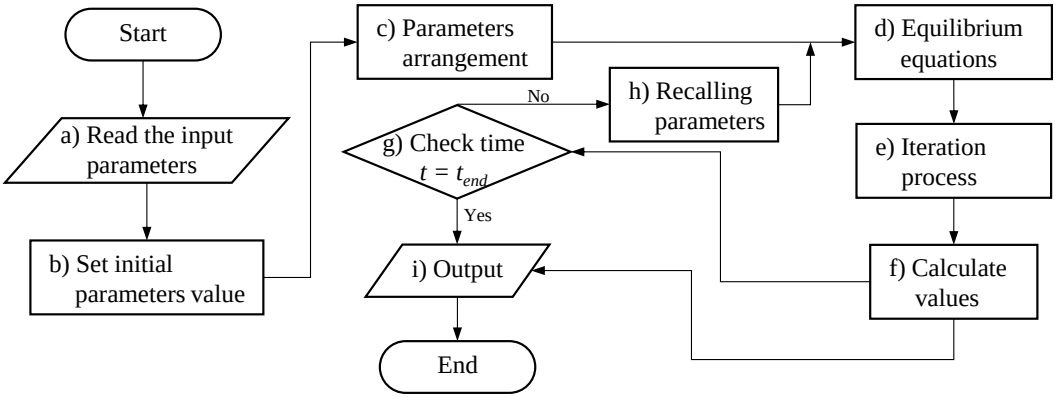

Figure 2. Algorithm of VB syntax implemented for simulation with NTC model in the present study

The algorithm newly implemented into VB syntax consists of nine parts as shown in Figure 2. Part a) is to record the material properties and the simulation history parameters. Next, in Part b), all the variables used in the simulation are initialized with zero. Then, in Part c), all the parameters are arranged such that they are ready for iteration process, that is, they are properly arranged to make the source code easy to edit. After that, Part d) is to set up the equilibrium equation (described in Section 3.2) that suits the specified simulation mode (e.g., Tables 2 and 3). Part e), which is the iteration process, is to find the root value of $\dot{\varepsilon}^{ir}_{[i+1]}$ that makes convergence of the equilibrium equation. The limit value of iteration step and iteration precision can be set via MS Excel interface (Figure 3). Then, Part f) is to calculate all the other variables from the obtained $\dot{\varepsilon}^{ir}_{[i+1]}$ and record them into the "Result.txt" file. Next, in Part g), it is to check whether the "time" at the stage $i + 1$ is equal to the end time (t_{end}). If the condition in Part g) is false, Part h) is implemented to recall the necessary variables at stage $i + 1$ from Part f), and then set as for stage i for the iteration process. Upon the condition in Part g) is true, Part i) is to finalize the "Result.txt" file and terminate the program.

3.3 *Input parameters and simulation steps*

3.3.1 *Input parameters*

There are two types of input parameters: i) material properties; and ii) simulation history parameters. The material properties, which are according to the elastic, inviscid, and viscous bodies (Figure 1a) as described in Sections 2.1, 2.2, and 2.3, respectively, can be determined by sophisticated tensile loading tests (e.g., Hirakawa et al. 2003, Kongkitkul et al. 2004, 2007a, 2012). The simulation history parameters can be prepared by the measured time history of either total strain rate, creep period, or stress relaxation period for ML, SL, or SR mode, respectively. Simulation of load-strain-time behavior subjected to complex loading histories can be done by combination of simulation-history parameters of ML, SL and SR modes. In this paper, both the material properties and simulation history parameters for respective simulations were taken from the work by Hirakawa et al. (2003). The material properties are tabulated in Table 1. Ta-

bles 2a and 2b show the simulation history parameters used in the simulation of HDPE and PET geogrids used in the present study. Note that the numbers for the "Event" column of 1, 2, and 3 in Tables 2a and 2b stand for ML, SL, and SR modes, respectively.

Table 1. Material properties of HPDE and PET geogrids implied in the present study

NTC Component	Symbol	HDPE	PET
Elastic	k_{eq0}	15 kN/m/%	25 kN/m/%
	b	0	0
	T_0	1 kN/m	1 kN/m
Viscous (viscosity function)	α	1.6	0.4
	m	0.085	0.12
	$\dot{\varepsilon}_r^{ir}$	2.10E-04 %/s	1.00E-05 %/s
Viscous (decay function)	$r(\varepsilon^{ir})$	Contant	Varies
	r_i	1	1
	r_f	1	0.15
	c	1 %	0.4 %
	n	0	0.6

NTC Component	Symbol	HDPE	PET
Viscous (combined parameter)	$\theta(\varepsilon^{ir})$	Contant	Constant
	θ_i	1	0.8
	θ_f	1	0.8
	n_θ	0	0
	$\varepsilon_{0.\theta}^{ir}$	1 %	1 %
Inviscid	a_1	13.39596	4.99898
	a_2	-4.96765	-1.17026
	a_3	1.1236	0.14392
	a_4	-0.11691	-0.0081
	a_5	0.0045	0.00023
	a_6	0	-2.7814E-06
	a_7	0	0
	a_8	0	0
	a_9	0	0

Table 2. a) (left) Combination of simulation history parameters for HDPE geogrid in the present study; and b) (right) Combination of simulation history parameters for PET geogrid in the present study

Event	t_{int}(sec)	t_{end}(sec)	Value
1	0	128	0.005
1	128	3323	0.00031
1	3323	3367	0.02615
1	3367	7973	0.00052
2	7973	53075	0
1	53075	57100	0.00036
1	57100	57553	0.00336
5	57553	100806	0
1	100806	101266	0.00182

Event	t_{int}(sec)	t_{end}(sec)	Value
1	0	143	0.01099
1	143	1148	0.0014
1	1148	1254	0.01347
1	1254	9927	0.000125
1	9927	10065	0.01304
1	10065	11100	0.0012
2	11100	14709	0
1	14709	17690	0.00097
5	17690	21300	0
1	21300	24795	0.00085
1	24795	25134	0.00831

3.3.2 *Simulation steps*

The present study adapts some features of user interface from the original computer program developed by Nishi (2002) in Microsoft Visual C++. Simulation steps of the VB program developed in the present study can be explained as follows.

i) Enter the values of material properties on MS Excel interface as shown in Figure 3, prepare a "ControlFile.txt" file that records the combination of simulation history parameters (Tables 2a and 2b) and place in the same folder as for the VB program.

ii) Press "Run" button on MS Excel worksheet interface so that the VB will operate.

iii) Simulation result is automatically created as "Result.txt" file in the same folder as for the VB program.

iv) The "Result.txt" file can be imported to MS Excel interface by using "Paste data" button on MS Excel worksheet. The simulation result is reported with 17 columns. In addition, this result can be deleted by pressing at "Clear" button.

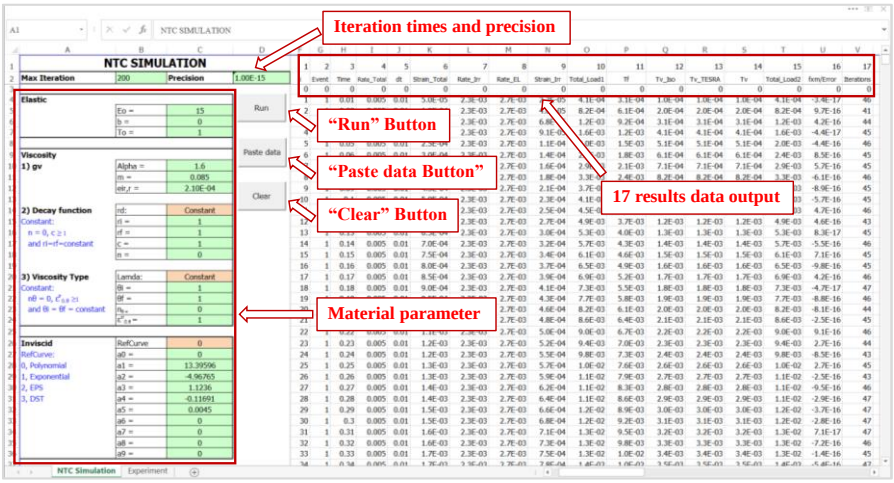

Figure 3 MS Excel interface for simulation with VB program developed in the present study

4 SIMULATION

Figure 4a compares the tensile load-strain relations of HDPE geogrid among the experiment, the simulation by Hirakawa et al. (2003), and the simulation by VB in the present study. Similarly, Figure 5a compares the tensile load-strain relations of PET geogrid. Figure 4b compares time histories of creep strain increment (stages *h* to *i* in Figure 4a), among the experiment, the simulation by Hirakawa et al. (2003), and the simulation by VB in the present study, for HDPE geogrid. Similarly, Figure 5b compares time histories of creep strain increment (stages *i* to *j* in Figure 5a), for PET geogrid. It can be clearly seen that not only all the rate-dependent tensile load-strain behaviours but also time histories of creep strain increment during SL and tensile load decrement during SR are successfully simulated by the VB newly developed in the present study.

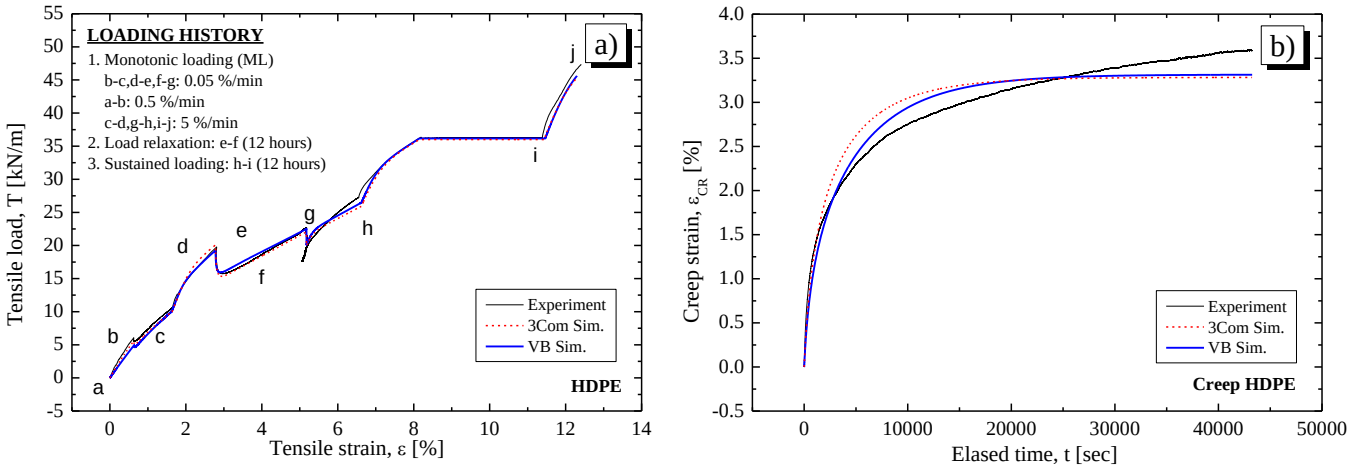

Figure 4. a) (left) Tensile load-strain relations; and b) (right) Creep strain-time relations for HDPE

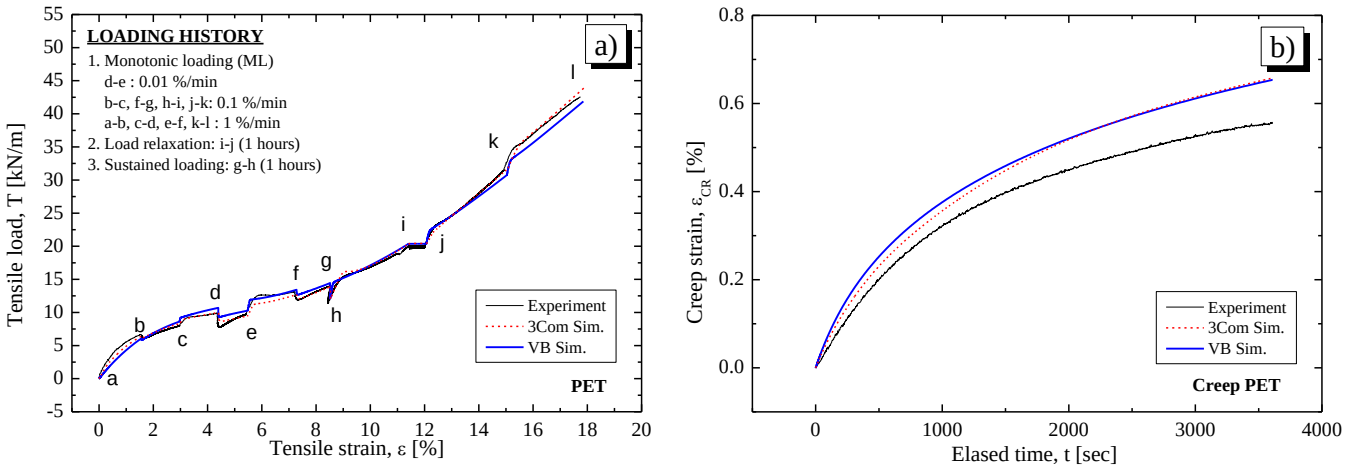

Figure 5. a) (left) Tensile load-strain relations; and b) (right) Creep strain-time relations for PET

5 SUMMARY

Most polymer geosynthetic reinforcement exhibit rate-dependent tensile load-strain behaviours due to the material viscous property. Among various types of viscosity, Isotach type is found relevant with most polymer types, while Combined type with polyester. A non-linear three-component model was successfully used to simulate the rate-dependent tensile load-strain behaviours of geosynthetic reinforcement, taking into account not only various viscosity types but also the dependency of the elastic stiffness with the tensile load. In the present study, equilibrium equations for various simulation modes including: monotonic loading (ML), sustained loading (SL), and stress relaxation (SR), are detailed and explained. These equations are used for iteration process of the root value of irreversible strain increment at the current stage in the simulation. Then, the source code for the simulation was newly developed in VB source code built-in MS Excel. The simulation procedures as well as the algorithm and working principles are also extensively explained. Simulations were performed on two tensile loading test results, and compared with the simulation results by the previous research. The new simulation results showed a very good agreement with both the experiment and previous simulation results. Thus, it can be concluded that, with the newly developed VB source code, the rate-dependent load-strain behaviours observed during constant strain rate ML, SL and SR in experiments can be successfully simulated by the algorithm developed in this study.

6 ACKNOWLEDGEMENT

The authors would like to express their gratitude for financial support from King Mongkut's University of Technology Thonburi (KMUTT) through The Petchra Pra Jom Klao PhD scholarship under contract Grant No. 3/2559.

REFERENCES

Chantachot, T., Kongkitkul, W. & Tatsuoka, F. 2016. Load-strain-time behaviours of two polymer geogrids affected by temperature. International Journal of GEOMATE, Vol. 10(21), pp. 1869-1876.

Di Benedetto, H., Tatsuoka, F. & Ishihara, M. 2002. Time-dependent shear deformation characteristics of sand and their constitutive modelling. Soils and Foundations, Vol. 42(2), pp. 1-22.

Ezzein, F.M., Bathurst, R.J. & Kongkitkul, W. 2015. Nonlinear load–strain modeling of polypropylene geogrids during constant rate of strain loading. Polymer Engineering and Science, Vol. 55(7), pp. 1617-1627.

Hirakawa, D., Kongkitkul, W., Tatsuoka, F. & Uchimura, T. 2003. Time-dependent stress–strain behaviour due to viscous properties of geogrid reinforcement. Geosynthetics International, Vol. 10(6), pp. 176-199.

Ishihara, M. (2000). Time-dependent deformation characteristics of sand and its modelling. M.Eng thesis, University of Tokyo, Tokyo, Japan, (in Japanese).

Kongkitkul, W., Hirakawa, D., Tatsuoka, F. & Uchimura, T. 2004. Viscous deformation of geosynthetic reinforcement under cyclic loading conditions and its model simulation. Geosynthetics international, Vol. 11(2), pp. 73-99.

Kongkitkul, W., Hirakawa, D. & Tatsuoka, F. 2007a. Viscous behaviour of geogrids; experiment and simulation. Soils and Foundations, Vol. 47(2), pp. 265-283.

Kongkitkul, W. & Tatsuoka, F. 2007b. A theoretical framework to analyse the behaviour of polymer geosynthetic reinforcement in temperature-accelerated creep tests. Geosynthetics International, Vol. 14(1), pp. 23-38.

Kongkitkul, W., Tatsuoka, F., Hirakawa, D., Sugimoto, T., Kawahata, S. & Ito, M. 2010. Time histories of tensile force in geogrid arranged in two full-scale high walls. Geosynthetics International, Vol. 17(1), pp. 12-33.

Kongkitkul, W., Tabsombut, W., Jaturapitakkul, C. & Tatsuoka, F. 2012. Effects of temperature on the rupture strength and elastic stiffness of geogrids. Geosynthetics International, Vol. 19(2), pp. 106-123.

Kongkitkul, W., Chantachot, T. & Tatsuoka, F. 2014. Simulation of geosynthetic load–strain–time behaviour by the non-linear three-component model. Geosynthetics International, Vol. 21(4), pp. 244-255.

Nishi, T. (2002). Time effects on deformation and strength characteristics of geomaterials and its modelling. M.Eng thesis, University of Tokyo, Tokyo, Japan.

Peng, F.L., Li, F.L., Tan, Y. & Kongkitkul, W. 2010. Effects of loading rate on viscoplastic properties of polymer geosynthetics and its constitutive modeling. Polymer Engineering & Science, Vol. 50(3), pp. 550-560.

Shi, W., Peng, F. & Kongkitkul, W. 2016. FE simulation of rate-dependent behaviours of polymer geosynthetic reinforcements for an estimation of mobilized tensile force in a reinforced soil. Computers and Geotechnics, Vol. 80, pp. 49-58.

Tatsuoka, F., Ishihara, M., Di Benedetto, H. & Kuwano, R. 2002. Time-dependent shear deformation characteristics of geomaterials and their simulation. Soils and foundations, Vol. 42(2), pp. 103-129.

Tatsuoka, F., Di Benedetto, H., Enomoto, T., Kawabe, S. & Kongkitkul, W. 2008. Various viscosity types of geomaterials in shear and their mathematical expression. Soils and Foundations, Vol. 48(1), pp. 41-60.